Supporting Information

A Luminescent Amine-Functionalized Metal-Organic Framework Conjugated with Folic Acid as a Targeted Biocompatible pH-Responsive Nanocarrier for Apoptosis Induction in Breast Cancer Cells

Reza Abazari,[†] Farangis Ataei,[‡] Ali Morsali,*[,†] Alexandra M. Z. Slawin,[§] and Cameron L. Carpenter-Warren[§]

[†]Department of Chemistry, Faculty of Basic Sciences, Tarbiat Modares University, Tehran, 14115–175, Iran

[‡]Department of Biochemistry, Faculty of Biological Sciences, Tarbiat Modares University, Tehran, 14115–175, Iran

[§]School of Chemistry, University of St Andrews, St Andrews, Fife, KY16 9ST, UK

E-mail: morsali_a@modares.ac.ir

Collection and reduction of X-ray data. X-ray diffraction data was collected at 125 K using a Rigaku SCXmini CCD diffractometer with a SHINE monochromator [Mo Kα radiation (λ = 0.71075 Å)]. Intensity data were collected using ω steps accumulating area detector images spanning at least a hemisphere of reciprocal space. All data were corrected for Lorentz polarization effects. A multiscan absorption correction was applied by using CrysAlisPro[1] Structures were solved by dual space methods (SHELXT) and refined by full-matrix least-squares against F^2 (SHELXL-2013).[2] Non-hydrogen atoms were refined anisotropically, and hydrogen atoms were refined using a riding model, with the exception of the N-H's, which were refined freely. All calculations were performed using Olex 2.[3] The occupancy of the second DMF molecule was set to 0.5, in order to obtain consistent thermal parameters - the formula reflects this. Selected crystallographic data are presented in Table S1.

Figure S1. Light microscope image of bulk NH_2-Eu:TMU-62 crystals.

Figure S2. Fluorescence microscope image of bulk NH_2-Eu:TMU-62 crystals.

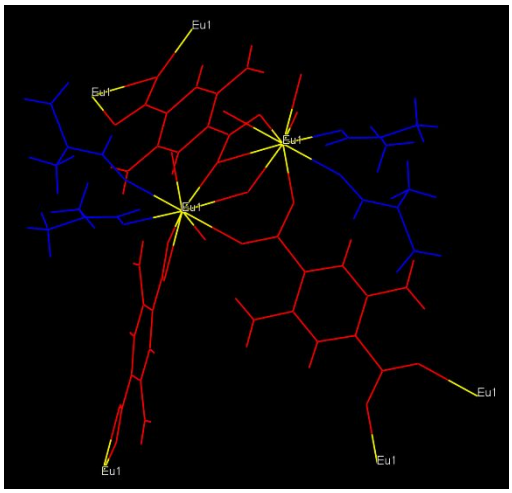

Figure S3. The coordination environment of the NH_2-Eu:TMU-62 (2-ATA ligand: red; DMF: blue; and Eu: yellow).

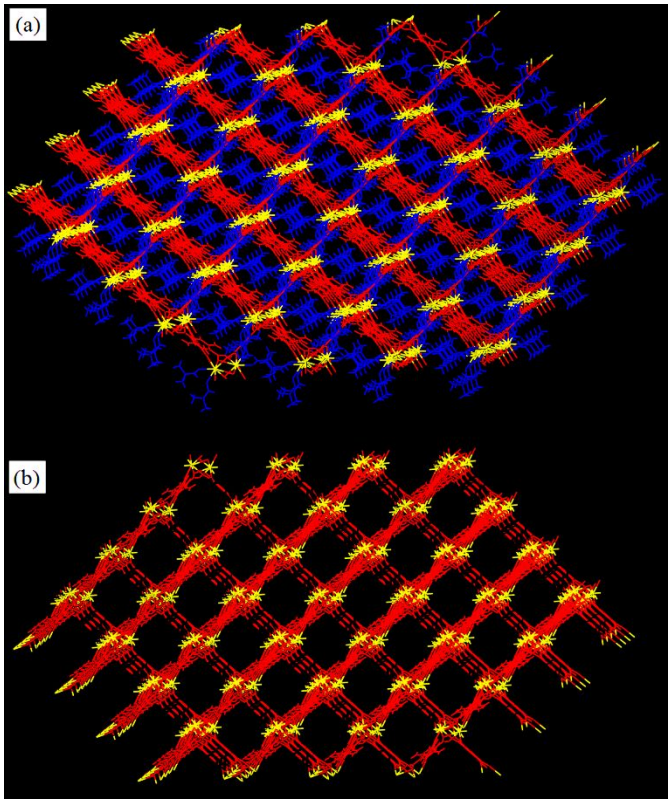

Figure S4. The pore geometry of the 3D structure of the NH_2-Eu:TMU-62 along the *c* axis. (a) With coordinated DMF molecules and (b) activated NH_2-Eu:TMU-62.

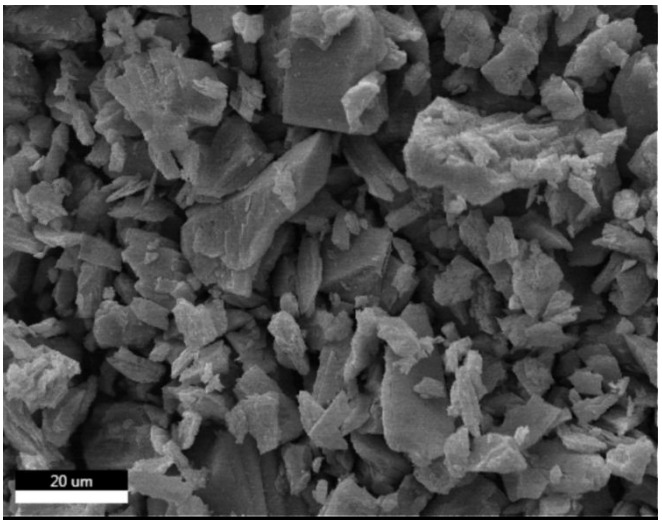

Figure S5. The FE-SEM image of the NH_2-Eu:TMU-62 crystals.

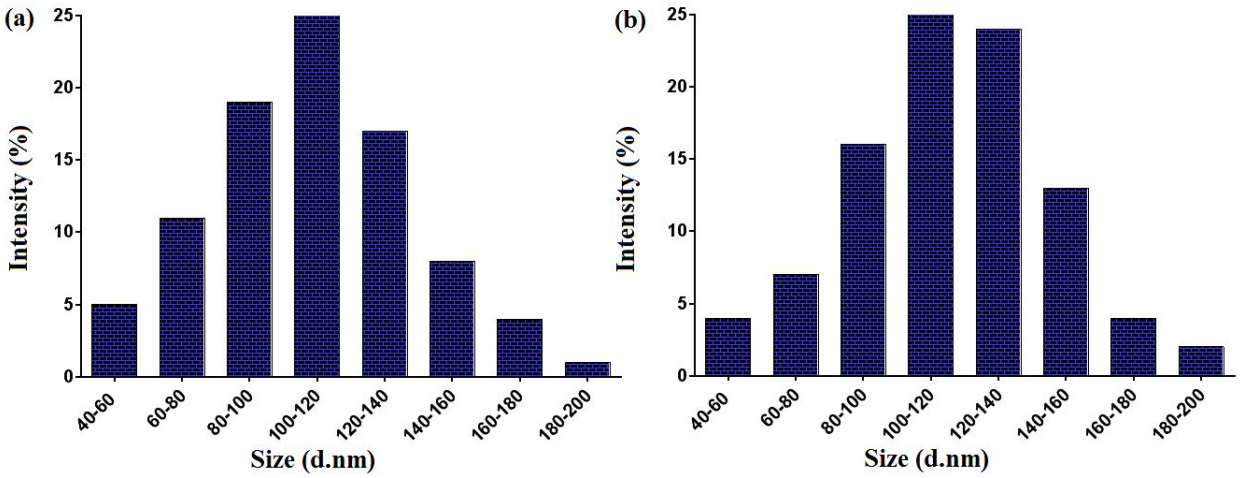

Figure S6. Particle size distribution of the FOLA@NH_2-Eu:TMU-62 in water (a) and PBS (b).

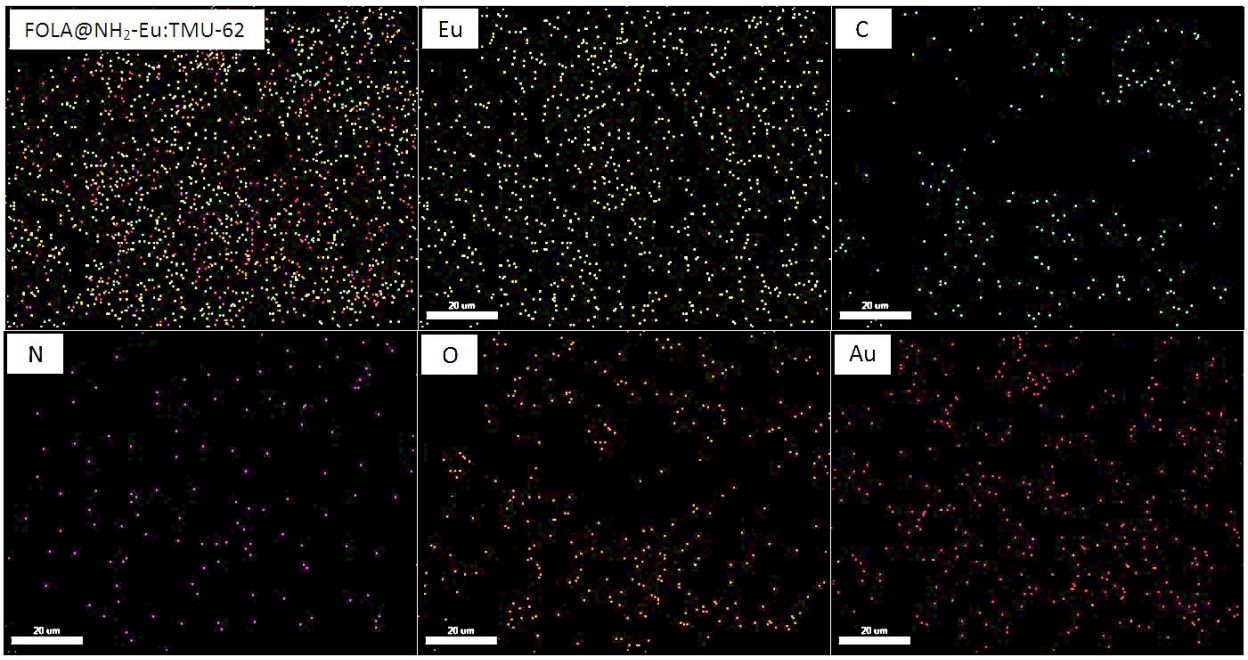

Figure S7. The elemental mapping of the FOLA@NH_2-Eu:TMU-62.

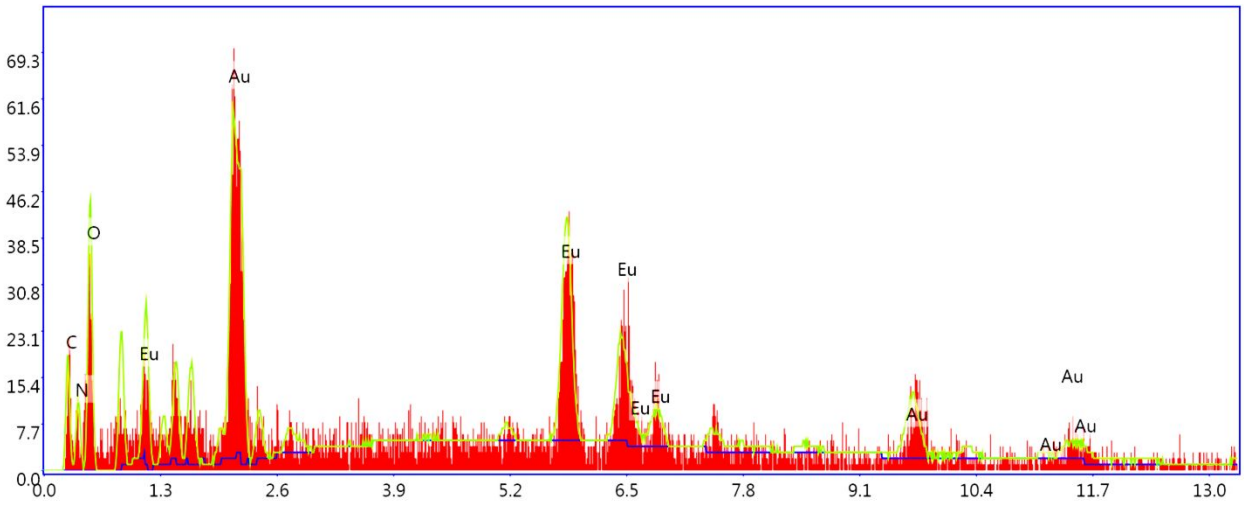

Figure S8. EDS analysis of the synthesized FOLA@NH_2-Eu:TMU-62.

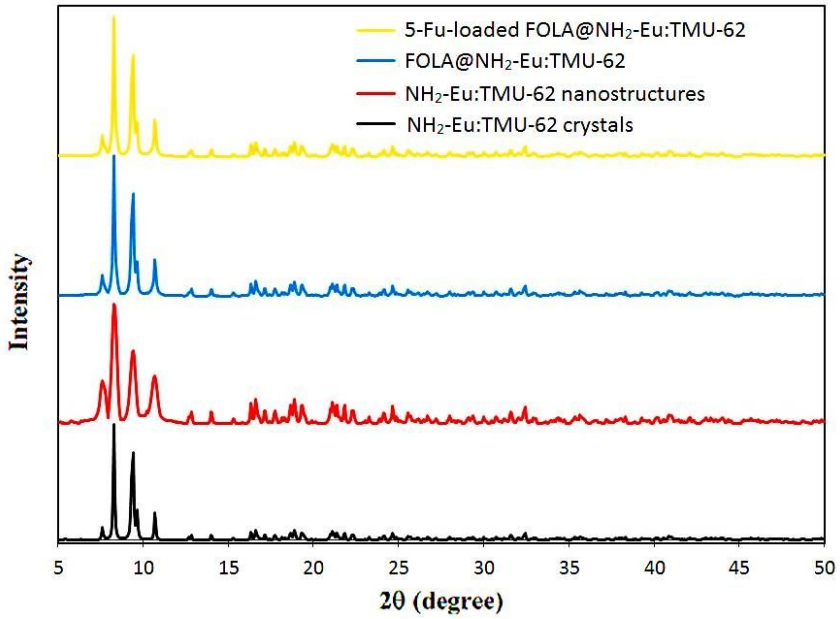

Figure S9. The XRD patterns of the NH_2-Eu:TMU-62 structure simulated from the single crystal X-ray data (black line), the NH_2-Eu:TMU-62 nanostructures synthesized via the conventional ball mill (red line), the FOLA@NH_2-Eu:TMU-62 (blue line), and the loaded FOLA@NH_2-Eu:TMU-62 with 5-Fu drug (orange line).

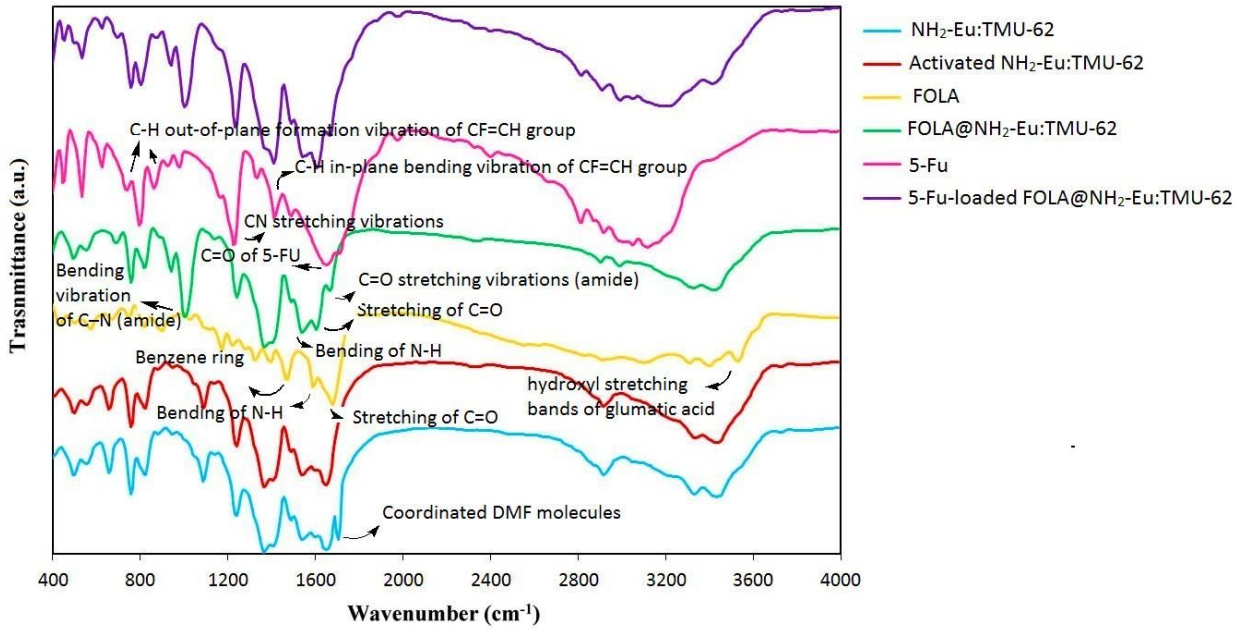

Figure S10. The FT-IR spectra of the NH_2-Eu:TMU-62 (blue line), activated NH_2-Eu:TMU-62 (red line), FOLA (orange line), FOLA@NH_2-Eu:TMU-62 (green line), 5-Fu (pink line), and 5-Fu-loaded FOLA@NH_2-Eu:TMU-62 (purple line).

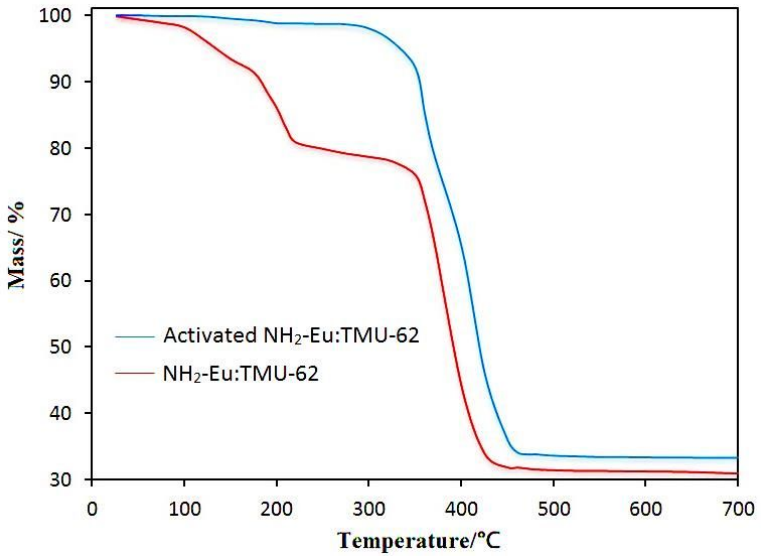

Figure S11. Thermogravimetric analysis of the NH_2-Eu:TMU-62 single crystals synthesized via the hydrothermal method (red line) and the NH_2-Eu:TMU-62 sample activated under vacuum at 140 ℃ for 24 h (blue line).

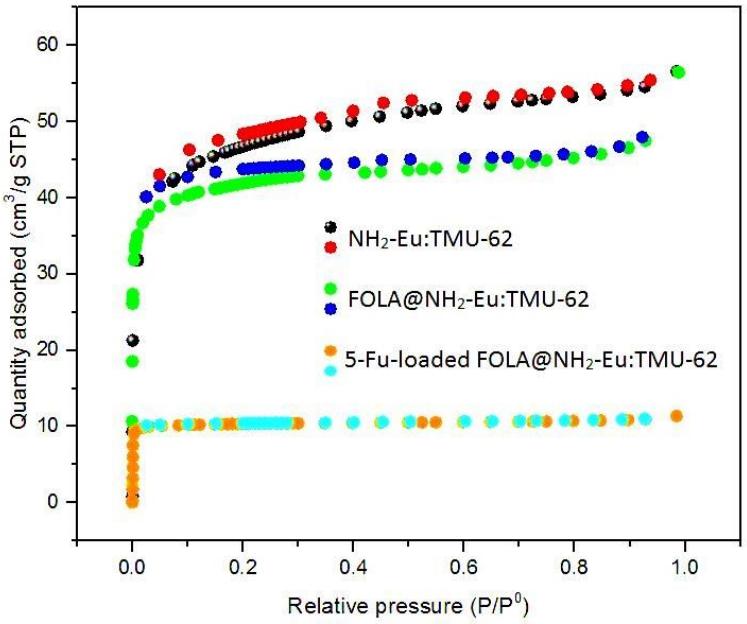

Figure S12. The N_2 adsorption-desorption isotherms of NH_2-Eu:TMU-62, FOLA@NH_2-Eu:TMU-62, and 5-Fu-loaded FOLA@NH_2-Eu:TMU-62 collected at 77 K.

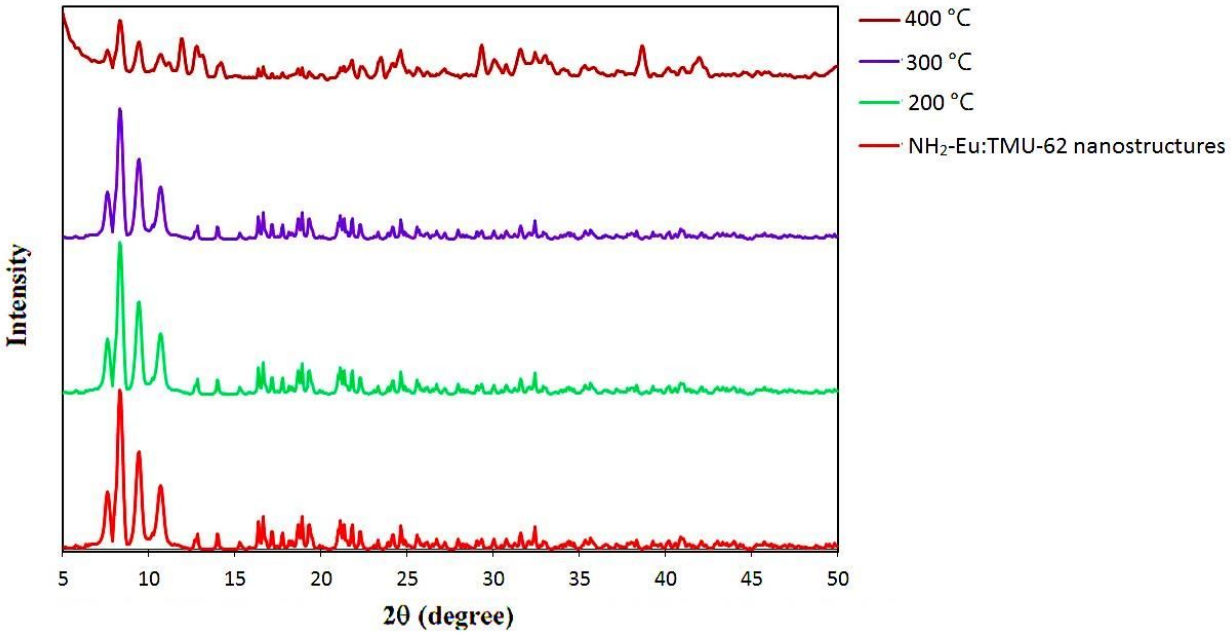

Figure S13. The PXRD patterns of the NH_2-Eu:TMU-62 nanostructures (red line); and the NH_2-Eu:TMU-62 nanostructures calcined in air at 200 °C (green line), 300 °C (purple line), and 400 °C (brown line).

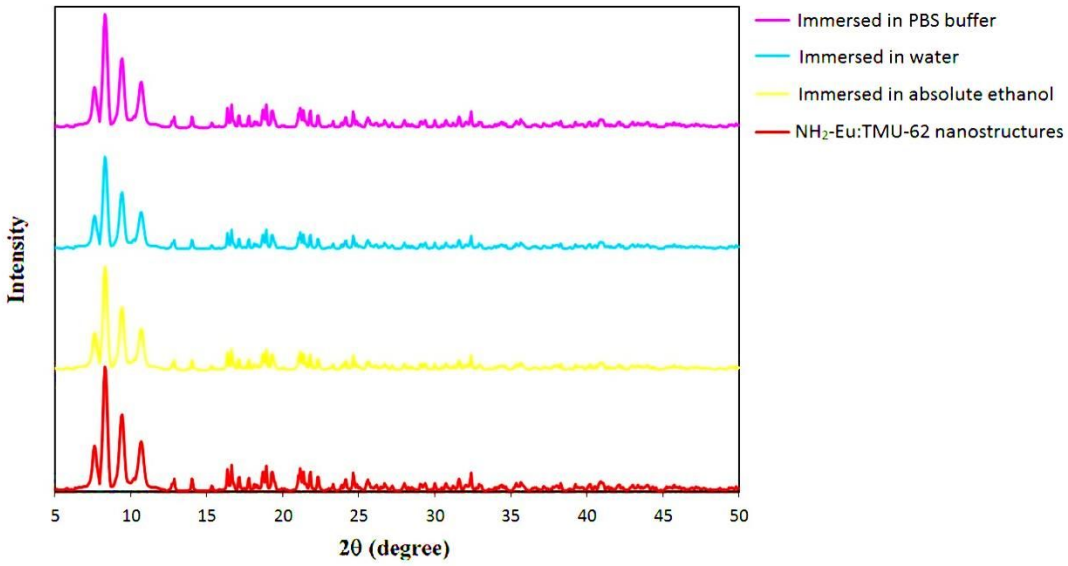

Figure S14. The PXRD patterns of the NH_2-Eu:TMU-62 nanostructures (red line); and the NH_2-Eu:TMU-62 nanostructures immersed in absolute ethanol (yellow line), water (blue line), and PBS buffer (pink line).

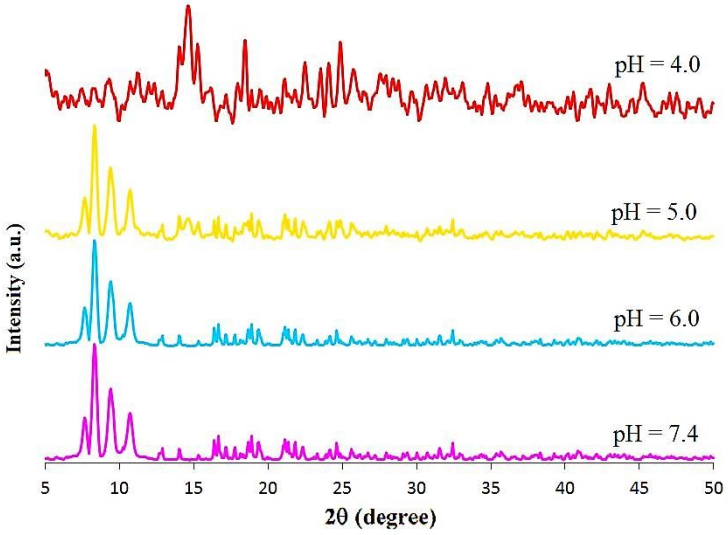

Figure S15. The PXRD patterns of FOLA@NH_2-Eu:TMU-62 carrier in the PBS solution at different pHs.

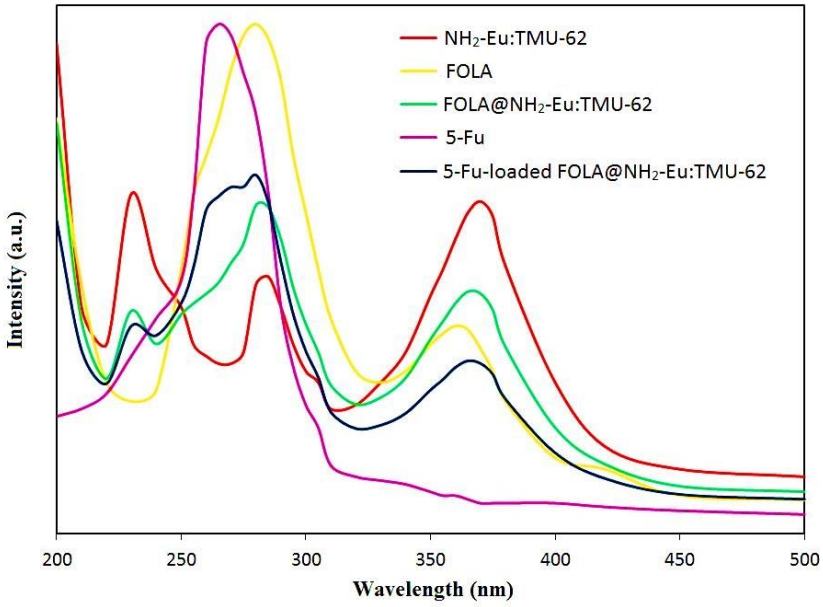

Figure S16. UV–visible absorption spectra of the NH_2-Eu:TMU-62 (red line), FOLA (orange line), FOLA@NH_2-Eu:TMU-62 (green line), 5-Fu (pink line), and 5-Fu-loaded FOLA@NH_2-Eu:TMU-62 (dark blue).

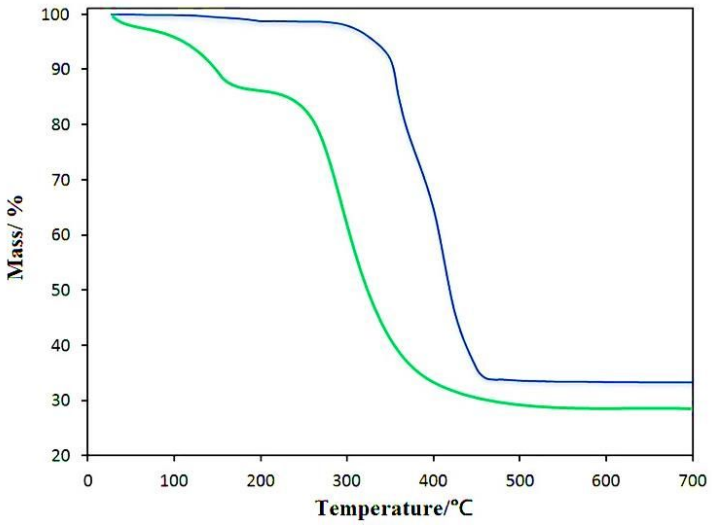

Figure S17. Thermogravimetric analysis of the NH_2-Eu:TMU-62 (blue line) and FOLA@NH_2-Eu:TMU-62 (green line).

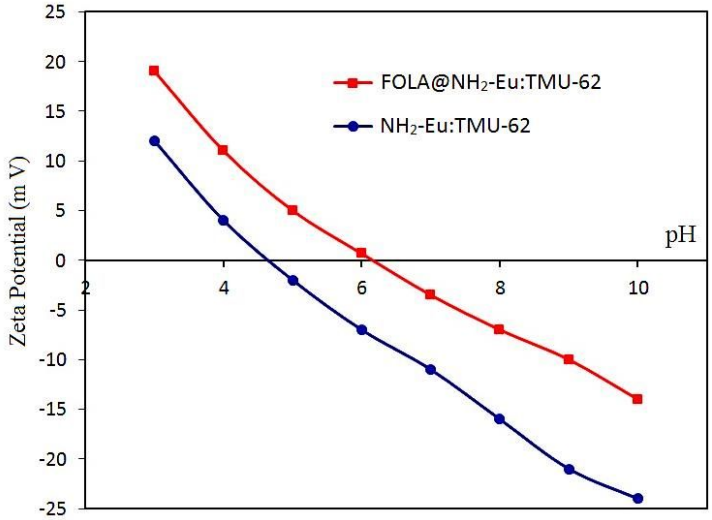

Figure S18. Variation of zeta-potential of NH_2-Eu:TMU-62 (blue line) and FOLA@NH_2-Eu:TMU-62 (red line) as a function of pH.

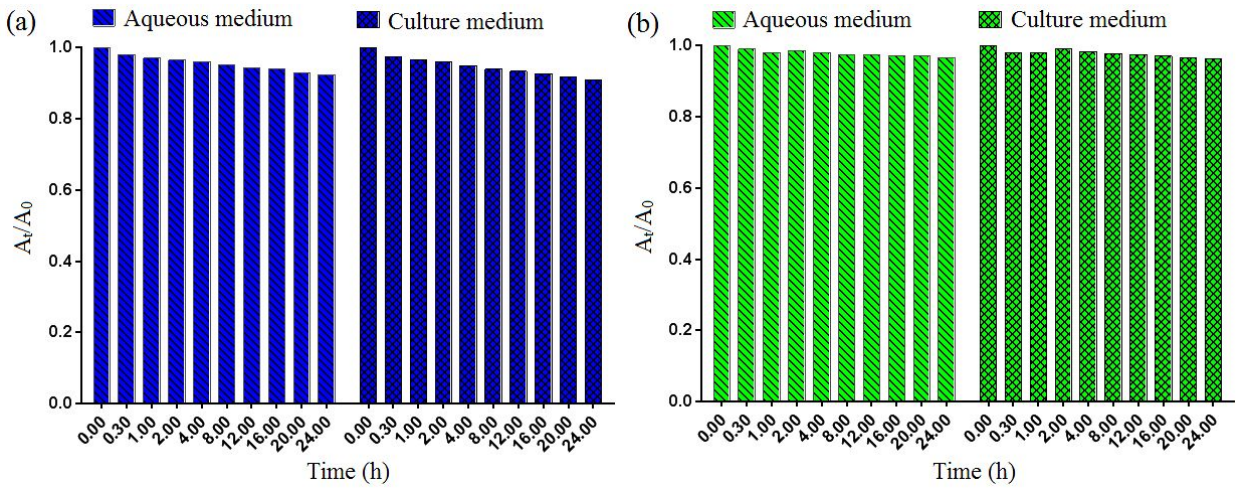

Figure S19. Normalized UV absorbance (A_t/A_0) vs. time plots of (a) the NH_2-Eu:TMU-62 and (b) and FOLA@NH_2-Eu:TMU-62 in aqueous and culture medium in different mediums (A_t = absorbance at time 't' and A_0 = Absorbance at t=0).

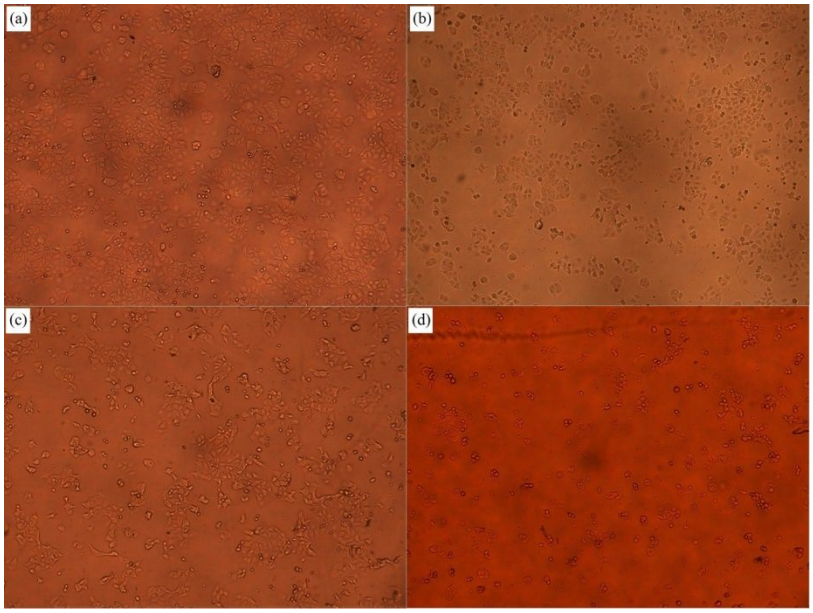

Figure S20. The morphological changes in the MCF-7 cells of the control group (a) and the cells exposed to the FOLA@NH_2-Eu:TMU-62 carrier (b), alone 5-Fu (c), and 5-Fu-loaded FOLA@NH_2-Eu:TMU-62 (d) at pH 7.4 for 24 h. Cell density reduction, irregular shapes and cellular shrinkage were observed by optical microscopy.

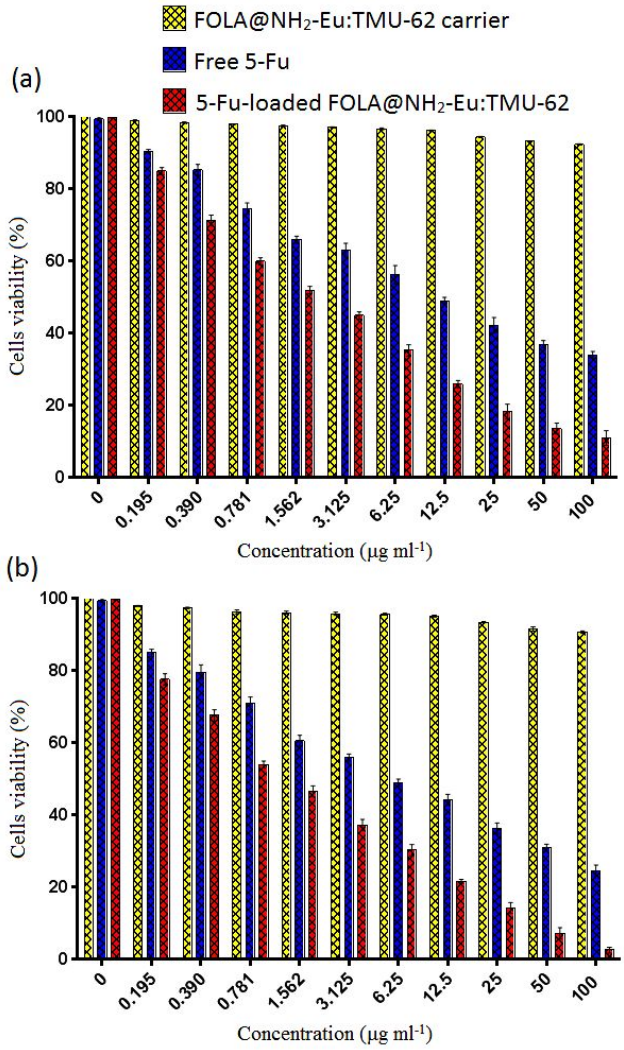

Figure S21. Comparison of the cytotoxic effect of the FOLA@NH_2-Eu:TMU-62 carrier, alone 5-Fu, and 5-Fu-loaded FOLA@NH_2-Eu:TMU-62 on cell viability of the MCF-7 cells incubated at pH 7.4 in the presence of various concentrations of the samples for 24h (a) and 72h (b).

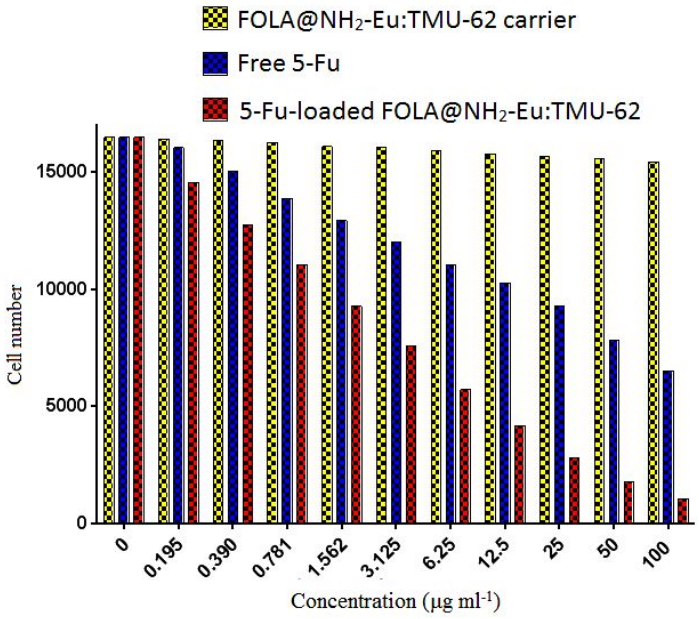

Figure S22. *In vitro* viability of the MCF-7 cells dyed with trypan blue and incubated at pH 7.4 for 24 h with various concentrations of the FOLA@NH_2-Eu:TMU-62 carrier, alone 5-Fu, and 5-Fu-loaded FOLA@NH_2-Eu:TMU-62.

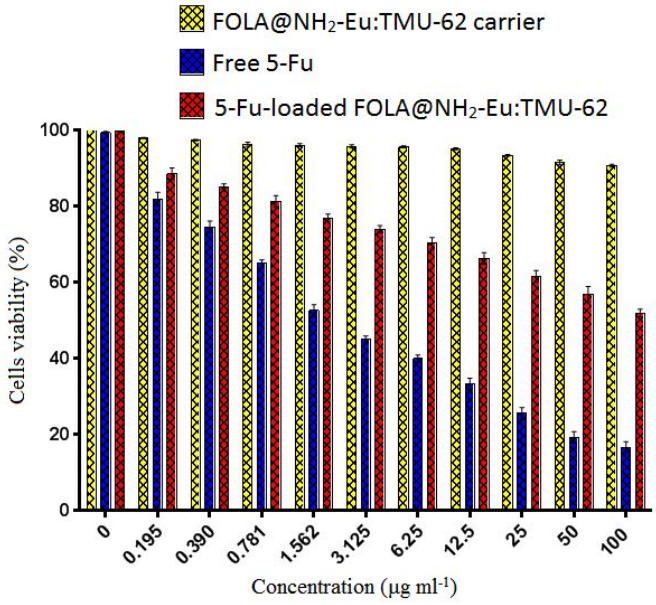

Figure S23. Comparison of the cytotoxic effect of the FOLA@NH_2-Eu:TMU-62 carrier, alone 5-Fu, and 5-Fu-loaded FOLA@NH_2-Eu:TMU-62 on cell viability of the MCF-10A cells incubated at pH 7.4 for 24h in the presence of various concentrations of the samples.

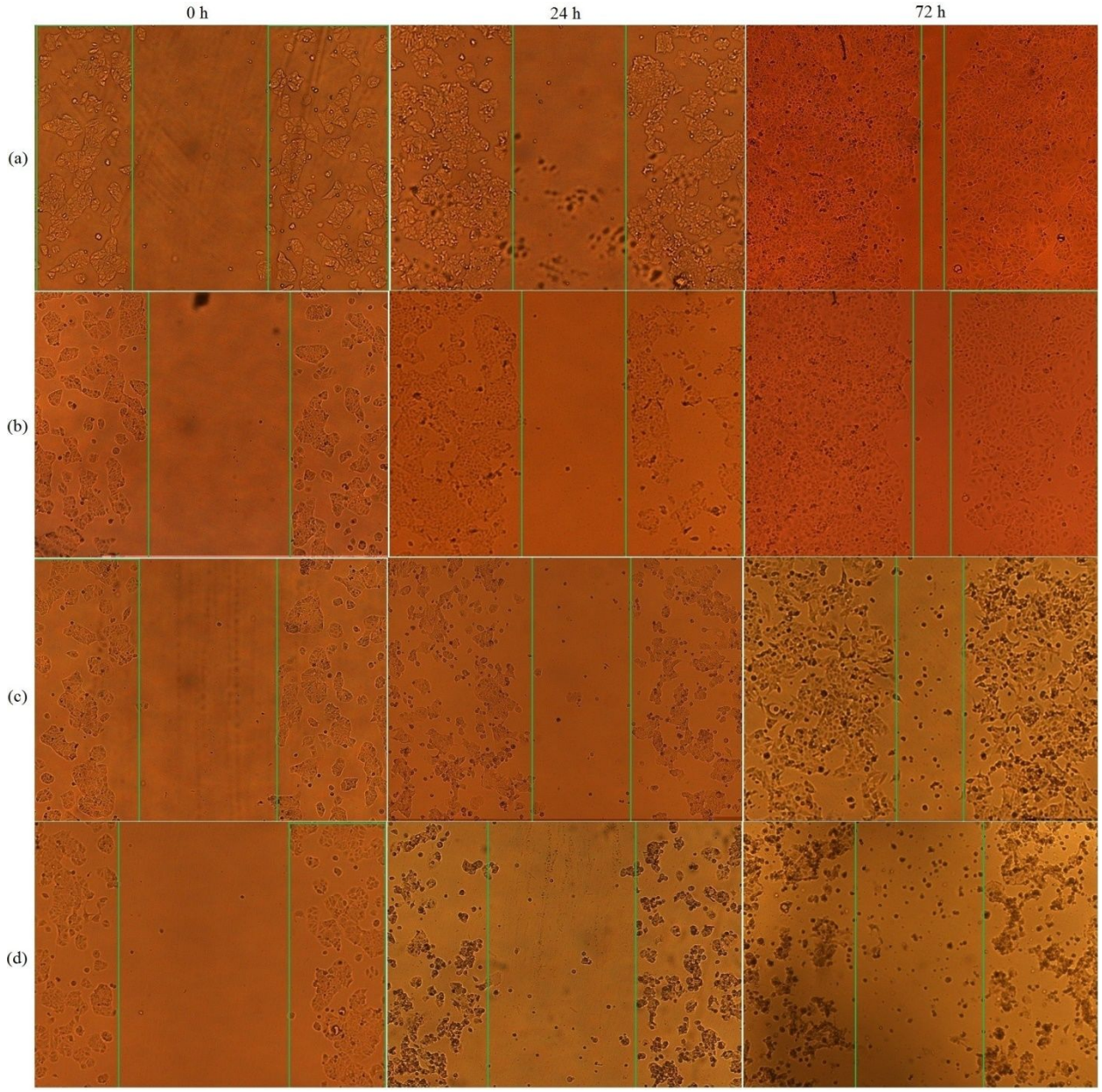

Figure S24. Optical microscopic images in migratory abilities of MCF-7 cells in wound healing assay at 0, 24 and 72h after the creation of wounds. (a) Control group, (b) FOLA@NH_2-Eu:TMU-62, (c) alone 5-Fu and (d) 5-Fu-loaded FOLA@NH_2-Eu:TMU-62.

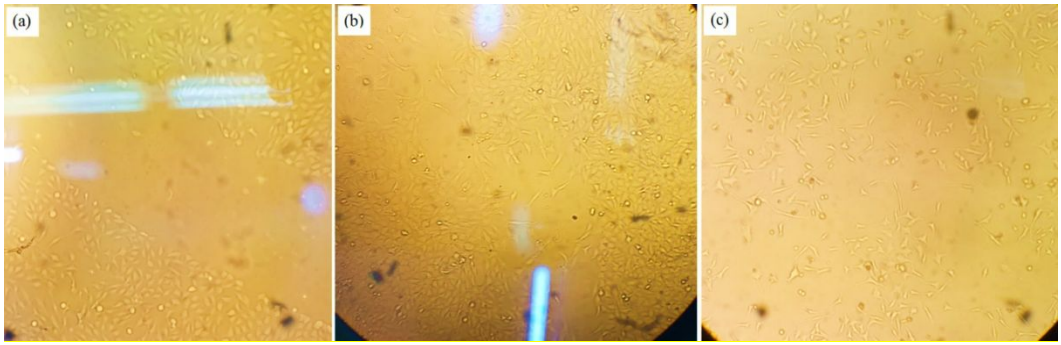

Figure S25. Optical microscopic images in migratory abilities of MCF-10A cells in wound healing assay at 72h after the creation of wounds. (a) Control group, (b) 5-Fu-loaded FOLA@NH_2-Eu:TMU-62 after 24 h, and (c) 5-Fu-loaded FOLA@NH_2-Eu:TMU-62 after 72 h.

Table S1. Quantitative apoptosis assay on the MCF-7 cell line using the Anexin-V/PI dual staining method in the framework of the flow cytometry method. The percentage of the viable, early apoptotic, late apoptotic and necrotic cells are presented as mean values (*n* = 3).

Treatment Group	Conc. (μg ml^{-1})	Viable cells (Q4%)	Early apoptotic cell (Q3%)	Late apoptotic cells (Q2%)	Necrotic cells (Q1%)	Cell death	Apoptotic cells (Q2% + Q3%)
Control group	1.562	88.20	1.37	7.07	3.35	11.80	8.44
FOLA@NH_2-Eu:TMU-62	1.562	76.50	0.65	15.20	7.65	23.50	15.85
Free 5-Fu	1.562	59.10	1.63	22.50	16.77	40.90	24.13
5-Fu-loaded FOLA@NH_2-Eu:TMU-62	1.562	38.50	35.9	25.50	0.011	61.50	61.4

Table S2. Crystal data and structure refinement for TMU-62.

Identification code	TMU-62
Empirical formula	$Eu_{0.33}$ $N_{1.17}$ $O_{2.75}$ C_6 $H_{6.83}$
Formula weight	189.48
Temperature/K	173
Crystal system	triclinic
Space group	P-1
a/Å	10.5035(7)
b/Å	11.2286(8)
c/Å	12.8073(12)
α/°	100.493(8)
β/°	110.554(6)
γ/°	100.335(6)
Volume/Å^3	1341.2(2)
Z	6
ρ_{calc}g/cm^3	1.407
μ/mm^{-1}	0.517
F(000)	562.86
Crystal size/mm^3	0.220
Radiation	Mo Kα (λ = 0.71075)
2Θ range for data collection/°	3.52 to 50.48
Index ranges	-12 ≤ h ≤ 12, -13 ≤ k ≤ 13, -15 ≤ l ≤ 15
Reflections collected	11818
Independent reflections	11818 [R_{int} = 0.0722, R_{sigma} = 0.1427]
Data/restraints/parameters	11818/258/307
Goodness-of-fit on F^2	1.136
Final R indexes [I>=2σ (I)]	R_1 = 0.0486, wR_2 = 0.1466
Final R indexes [all data]	R_1 = 0.0442, wR_2 = 0.1439
Largest diff. peak/hole / e Å^{-3}	1.712/-1.013

References

(1) *CrysAlisPro* v1.171.38.41. Rigaku Oxford Diffraction, Rigaku Corporation, Oxford, U.K. **2015**.

(2) Sheldrick, G. M. *Acta Crystallogr., Sect. A*. **2015**, *71*, 3.

(3) Dolomanov, O.V.; Bourhis, L.J.; Gildea, R.J.; Howard, J.A.K.; Puschmann, H. *J. Appl. Cryst*. **2009**, *42*, 339.